

**\*\*FULL TITLE\*\***  
*ASP Conference Series, Vol. \*\*VOLUME\*\*, \*\*YEAR OF PUBLICATION\*\**  
**\*\*NAMES OF EDITORS\*\***

## Dark Matter Substructure in Lensing Galaxies

Masashi Chiba,<sup>1</sup> Takeo Minezaki,<sup>2</sup> Kaiki T. Inoue,<sup>3</sup>  
 Nobunari Kashikawa,<sup>4</sup> Hirokazu Kataza,<sup>5</sup> Hajime Sugai<sup>6</sup>

<sup>1</sup>*Astronomical Institute, Tohoku University, Sendai, Japan*

<sup>2</sup>*Institute of Astronomy, University of Tokyo, Mitaka, Tokyo, Japan*

<sup>3</sup>*School of Science and Engineering, Kinki Univ., Higashi Osaka, Japan*

<sup>4</sup>*National Astronomical Observatory of Japan, Mitaka, Tokyo, Japan*

<sup>5</sup>*ISAS, JAXA, Sagami-hara, Kanagawa, Japan*

<sup>6</sup>*Department of Astronomy, Kyoto University, Kyoto, Japan*

**Abstract.** To set useful limits on the abundance of small-scale dark matter halos (subhalos) in a galaxy scale, we have carried out mid-infrared imaging and integral-field spectroscopy for a sample of quadruple lens systems showing anomalous flux ratios. These observations using Subaru have been successful for distinguishing millilensing by subhalos from microlensing by stars. Current status for our lensing analysis of dark matter substructure is reported.

### 1. Introduction

Recent high-resolution N-body simulations based on Cold Dark Matter (CDM) theory highlight a so-called missing satellite problem, i.e., CDM predicts the existence of more than several hundred dark satellites (or subhalos) in a galaxy-sized halo, in sharp contrast to the observed number of about 20 Milky Way satellites (e.g., Diemand et al. 2007 for recent studies). To clarify this issue, gravitational lensing offers us an invaluable insight into such numerous CDM subhalos that reside in lensing galaxies. In particular, anomalous flux ratios in lensed QSOs, namely those hardly reproduced by any lens models with a smooth density distribution, are of special interest, since lens substructures are able to cause such flux anomalies (e.g., Metcalf & Madau 2001; Chiba 2002).

Here, we report on our Subaru observations of a sample of quadruple lenses with anomalous flux ratios, based on mid-infrared imaging and integral-field spectroscopy. Mid-infrared imaging of lenses is advantageous because the flux is free from differential extinction among different images and it is also free from microlensing by stars. Integral-field spectroscopy provides both spatial and spectral information simultaneously on each lensed image. We select eight QSOs with four lensed images, PG1115+080, B1422+231, MG0414+0534, Q2237+030, H1413+117, HS0810+2554, and WFI2026–4536 for mid-infrared imaging, and RXJ1131–1231 for integral-field spectroscopy. We briefly report the results for PG1115+080 and B1422+231 (Chiba et al. 2005) and RXJ1131–1231 (Sugai et al. 2007); those for other targets will be published elsewhere (Minezaki et al. 2008 in preparation). We present new limits on substructure in the observed lensed systems and implications for a missing satellite problem are discussed.

## 2. Targets and Observations

PG1115+080 at redshift  $z_S = 1.72$  and B1422+231 at  $z_S = 3.62$  are lensed by foreground ellipticals at  $z_L = 0.31$  and  $0.34$ , respectively. The former lens system holds the closely separated pair of images A1 and A2 with a separation of  $0.''48$ , and this configuration emerges if the QSO is close to and inside a fold caustic provided by the lens (Figure 1). The latter shows the colinear, three highly magnified images, A, B, and C, and this configuration emerges if the QSO is close to and inside a cusp caustic. In such lens systems associated with a fold or cusp caustic, there exists a universal relation between the image fluxes, i.e.,  $A_2/A_1 = 1$  or  $(A+C)/B = 1$ , whereas the observed optical flux ratios violate these rules significantly,  $A_2/A_1 = 0.64 \pm 0.02$  and  $(A+C)/B = 1.50 \pm 0.01$ .

The mid-infrared imaging of PG1115+080 and B1422+231 was carried out on the nights of UT 2004 May 5 and 6, using the cooled mid-infrared camera and spectrometer (COMICS). The field of view is  $42'' \times 32''$  and the pixel scale is  $0.''129 \text{ pixel}^{-1}$ . We used the N11.7 filter, whose effective wavelength and bandwidth are  $\lambda_c = 11.67 \mu\text{m}$  and  $\Delta\lambda = 1.05 \mu\text{m}$ , respectively. The FWHM of PSF was  $0.''33$  at small airmass. The observed mid-infrared waveband corresponds to the near-infrared waveband in the rest frame, and its flux is dominated by thermal radiation from hot dust located at the innermost region of a dust torus. The inner radius of a dust torus, which is determined by the highest sublimation temperature of dust ( $T \sim 1800 \text{ K}$ ) and the UV luminosity of a QSO central engine, is generally much larger than Einstein radii of foreground stars, so that the observed mid-infrared flux is free from microlensing effects.

RXJ1131–1231 is unique in its low redshift of a source image  $z_S = 0.658$  lensed by an elliptical at  $z_L = 0.295$ . The lens shows three roughly co-linear images, A, B, and, C, being characteristic of a cusp singularity, where A is brightest (Figure 2). The observed flux ratios,  $(B+C)/A \simeq 2.1$  in the  $V$  band and  $2.2$  in the  $R$  band, deviate significantly from the rule  $(B+C)/A = 1$ .

Using the IFS mode of the Kyoto tridimensional spectrograph II (Kyoto 3DII), we observed RXJ1131–1231 on the night of UT 2005 February 8. The IFS mode uses an array of  $37 \times 37$  lenslets, enabling us to obtain spectra of  $\sim 10^3$  spatial elements. The spectral range from  $7300\text{\AA}$  to  $9150\text{\AA}$  was observed in each of two one-hour exposures. With the spatial sampling of  $0.''096 \text{ lenslet}^{-1}$ , the field of view of  $\sim 3''$  covered the three bright lensed images. We measured the emission-line fluxes of both the BLR  $H\beta$  and the NLR  $[\text{OIII}]\lambda\lambda 4959, 5007$  for images A, B, and C simultaneously. The  $H\beta$  and  $[\text{OIII}]$  lines are very close in wavelength, so that the effect of differential reddening between them is negligible.

## 3. Results

The mid-infrared images at  $\lambda = 11.7 \mu\text{m}$  of PG1115+080 and B1422+231 are presented in Figure 1. It is evident that the lensed images in concern, (A1, A2) and (A, B, C), respectively, are clearly detected and well separated from each other. The mid-infrared flux ratios are given as  $A_2/A_1 = 0.93 \pm 0.06$ ,  $B/A_1 = 0.16 \pm 0.07$ , and  $C/A_1 = 0.21 \pm 0.04$  for PG1115+080, and  $(A+C)/B = 1.51 \pm 0.06$ ,  $A/B = 0.94 \pm 0.05$ , and  $C/B = 0.57 \pm 0.06$  for B1422+231. This suggests that the mid-infrared flux ratio for  $A_2/A_1$  of PG1115+080 is consistent with the

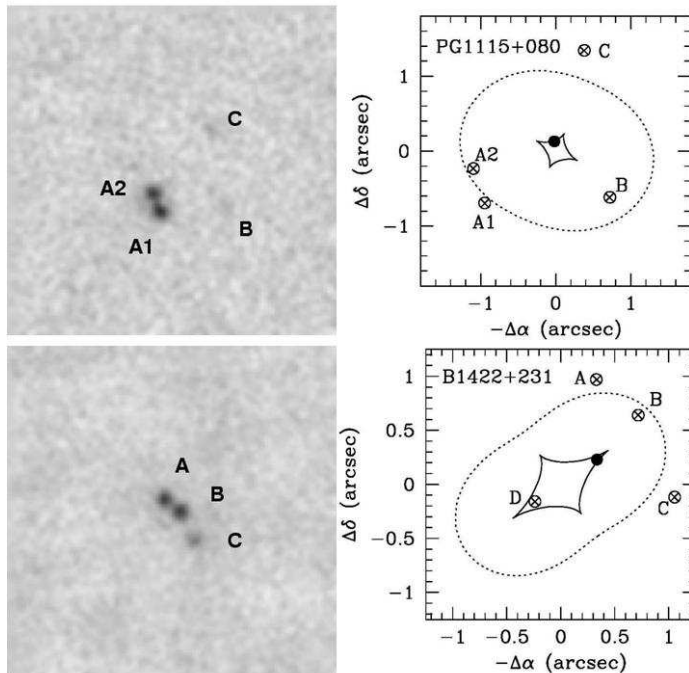


Figure 1. Left: Mid-infrared images at  $11.7 \mu\text{m}$  for PG1115+080 (top) and B1422+231 (bottom). The north is up and the east is left. Right: Smooth lens models for these systems, where solid and dotted lines denote the caustics and critical curves, respectively, and filled circles indicate the source positions.

prediction of a smooth lens model ( $\simeq 1$ ), while the optical flux ratio is much smaller ( $\simeq 0.65$ ), and that the mid-infrared flux ratios for (A, B, C) images of B1422+231 remain anomalous, contrary to the prediction of a smooth lens.

Based on the dust reverberation method for estimating the size of a dust torus (Minezaki et al. 2004), we obtain an angular size  $\theta_S$  of a source image as  $\theta_S \simeq 1 \times 10^{-4}$  arcsec and  $3.7 \times 10^{-4}$  arcsec for PG1115+080 and B1422+231, respectively. For PG1115+080, any substructure causing its optical anomalous flux ratio A2/A1 should have a small Einstein angle  $\theta_E$  compared to  $\theta_S$ , because its mid-infrared ratio remains unaffected. This suggests that a substructure mass inside  $\theta_E$ , denoted as  $M_E$ , should be smaller than  $20 M_\odot$ , being comparable to the mass of a star, i.e., microlensing causes an optical anomalous flux ratio. For B1422+231, the presence of flux anomaly even in mid-infrared waveband suggests  $M_E \gtrsim 200 M_\odot$ , i.e., lensing by a subhalo is most likely.

Figure 2 shows the Kyoto 3DII spectra of RXJ1131–1231 for three bright images A, B, and C. It is interesting to remark that images B and C in [OIII] show nearly the same fluxes relative to image A, as expected from a smooth model at its cusp singularity. Thus, the absence of substructure lensing effects on this NLR [OIII] sets important limits on the mass of any substructures along the line of sight, as  $M_E < 10^5 M_\odot$ . In contrast, the  $H\beta$  line emission, which originates from the BLR, shows an anomaly in the flux ratio between images B and C, i.e., a factor two smaller C/B ratio than predicted by smooth-lens

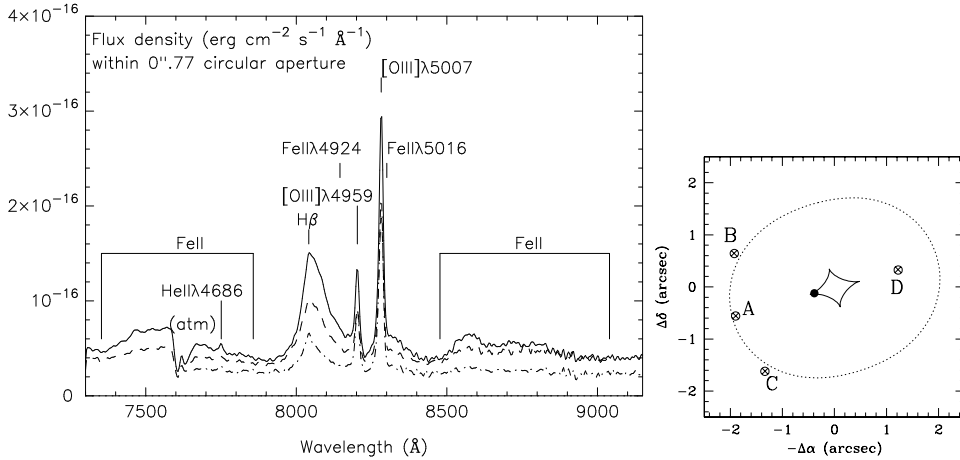


Figure 2. Left: Kyoto 3DII spectra of RXJ1131–1231 for image A (solid line), B (dashed line), and C (dot-dashed line), where each has been extracted with an 8-lenslet, i.e., a circular aperture with a diameter  $0''.77$ . Right: Smooth lens model for this lens system.

models. The ratio of A/B in the  $H\beta$  line is well reproduced. The anomalous C/B ratio for the  $H\beta$  line is caused most likely by microlensing of image C, with  $M_E \gtrsim 0.1 M_\odot$  for the mass of a substructure near image C. We have also found the slight difference of the  $H\beta$  line profile in image A from those in the other images, which suggests the presence of a small microlensing effect on image A.

#### 4. Prospects

In addition to the above lens systems, we have already observed, using COMICS, MG0414+0534, Q2237+030, H1413+117, and HS0810+2554, and the calibration and analysis are underway. Our final target for mid-infrared imaging of quadruple lenses, WFI2026–4536, is scheduled for observation using Gemini-South this year. Our preliminary statistical model implies that about 30 % of the lens systems (2 – 3 out of 8) show a flux anomaly with  $> 25$  %, if subhalos are modeled by tidally-truncated singular isothermal spheres with a mass function predicted by the N-body simulations. Once the concrete observational information for all of these targets is ready, we will be able to set a more reliable constraint on the abundance of CDM subhalos.

#### References

- Chiba, M. 2002, *ApJ*, 565, 17  
 Chiba, M. et al. 2005, *ApJ*, 627, 53  
 Diemand, J. et al. 2007, *ApJ*, 657, 262  
 Metcalf, R. B. & Madau, P. 2001, *ApJ*, 563, 9  
 Minezaki, T. et al. 2004, *ApJ*, 600, L35  
 Sugai, H. et al. 2007, *ApJ*, 660, 1016